Pergamon

Tetrahedron 56 (2000) 7561–7571

TETRAHEDRON

# Structures and Reactivities of 1-Oxo-cycloalkan-2-ylideneacetic Acids. A $^1$H NMR, Modelling and Photochemical Study

Stefano Ghelli,[a] M. Paola Costi,[b,*] Lucio Toma,[c] Daniela Barlocco[d] and Glauco Ponterini[a]

[a]*Dipartimento di Chimica, via Campi 183, 41100 Modena, Italy*
[b]*Dipartimento di Scienze Farmaceutiche, via Campi 183, 41100 Modena, Italy*
[c]*Dipartimento di Chimica Organica, via Taramelli 10, 27100 Pavia, Italy*
[d]*Istituto di Chimica Farmaceutica e Tossicologica, v.le Abruzzi 42, 20131 Milano, Italy*

Received 25 February 2000; revised 7 July 2000; accepted 20 July 2000

**Abstract**—Four 1-oxo-cycloalkan-2-ylideneacetic acids, differing in the size of the aliphatic ring and in the nature of the condensed unsaturated cycle, exhibit different reactivities towards hydrazine, leading in only one case to the desired tryciclic pyridazinone. The observed differences in behaviour cannot be ascribed to different configurations at the exocyclic double bond of the four acids: $^1$H NMR experiments, combined with UV photolysis, have shown that all compounds have been prepared in the *E* form and are stable in the absence of light and catalysts. The photochemically obtained *Z* isomers show an increasing tendency to form tricyclic lactones with increasing size of the aliphatic ring. A theoretical structural analysis of the *E* and *Z* isomers, the tricyclic lactones and some of the hypothetical intermediates of the reaction with hydrazine suggests the size of the aliphatic ring and the associated flexibility to be crucial in modulating the ability of these compounds to form tricyclic products. 

## Introduction

Since the appearance of the first benzocinnolinone in the literature,[1] the tricyclic pyridazinones of general structure **1** (see Scheme 1) have been widely employed in different fields of medicinal chemistry. In particular, cardiovascular,

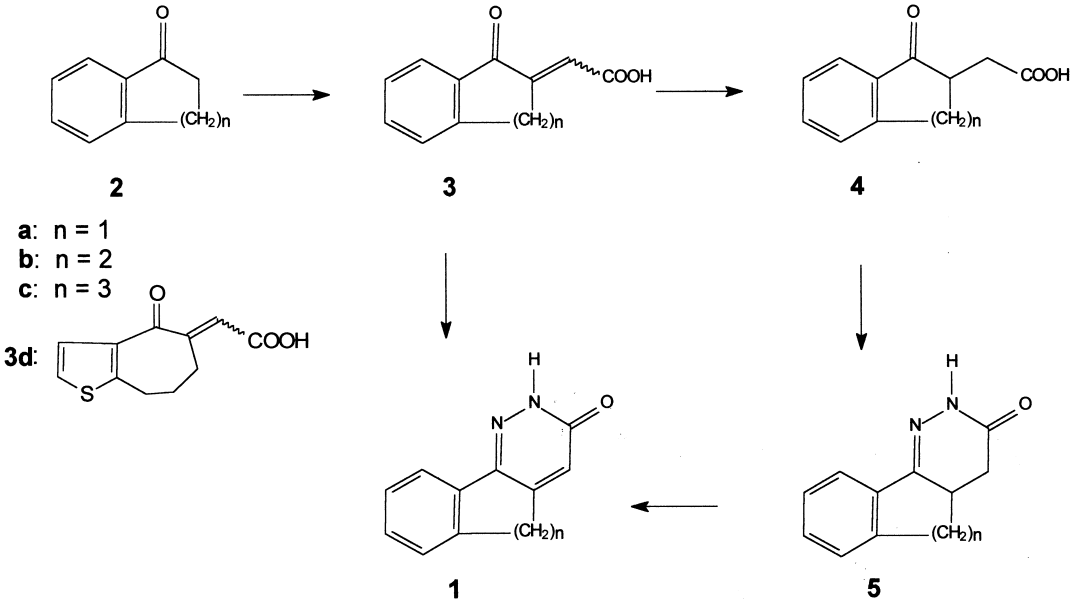


**Scheme 1.**

*Keywords*: tryciclic pyridazinone; arylidenecarboxyilic acids; UV photolysis; conformational studies.
* Corresponding author. Fax: +39-59-378560; e-mail: costimp@unimo.it

0040–4020/00/$ - see front matter 
PII: S0040-4020(00)00662-1

antisecretory, antiulcer, analgesic and antiinflammatory effects have been associated with these compounds.[2] Although more than one approach has been proposed for their synthesis,[3–6] the most common method is depicted in Scheme 1. Accordingly, the bicyclic ketone **2** is condensed with glyoxylic acid to give the unsaturated acid **3**, which is easily reduced to the corresponding **4**, which is then cyclised with hydrazine hydrate to the dihydroderivate **5**, and finally oxidised to **1**. However, while unsubstituted **5**, as well as its analogues carrying electron attracting groups on the phenyl moiety, could easily be dehydrogenated by bromine in acetic acid, analogues of compound **5** having electron donating groups on the phenyl ring underwent parallel bromination, leading to poor yields and complex reaction mixtures.[7] To overcome this side reaction, different oxidising systems were employed, e.g. sodium *m*-nitro-benzensulfonate in alkaline medium.[8,9] However, while this agent gave the desired **1b** and **c** from the corresponding **5b** and **c** in almost quantitative yields, in the case of **5a** no evidence of **1a** was detected in the reaction mixture.[10] Therefore, direct condensation of unsaturated **3** with hydrazine to give the corresponding **1** would be desirable. We therefore decided to explore the possibility of cyclising the indanylideneacetic acid **3a**, its higher homologues **3b** and **c** and the thiophene analogue **3d** with hydrazine hydrate. Indeed, compound **1a** was obtained by this route. On the other hand, reaction of compounds **3b**–**d** with hydrazine hydrate proved inefficient in giving compounds **1b**–**d** (Scheme 2).

These somewhat unexpected findings prompted us to investigate the reasons for different reactivities in the series **3a**–**d**. This could, in principle, result from a different configuration at the double bond, from geometrical constraints dictated by the different sizes of the aliphatic rings, or from electronic reasons. As an example of the latter, Lutz and co-workers found that while *cis*-β-aroyl-β-methylacrylic acids, which are structurally related to compounds **3**, easily cyclised to the corresponding lactones, the β-hydrogenated acids showed no tendency to cyclise under the same conditions.[11–12] To determine which of the possible causes was truly responsible for the different chemical behaviours of compounds **3**, we first carried out a structural investigation aimed at determining the configuration of the exocyclic double bond. This includes 1D and 2D $^1$H NMR extensive study, corroborated by modelling of the isolated molecules performed by the PM3 semiempirical approach. Subsequent photochemical experiments, monitored by UV–visible and $^1$H NMR spectra, have provided conclusive evidence about the structures of the starting isomers and have revealed different tendencies of compounds **3** to form cyclic products, also confirmed by PM3 modelling. An attempt at rationalising the observed reactivities of compounds **3a** and **b** towards hydrazine was finally made on the basis of calculated relative stabilities of the intermediates of two competitive reaction paths.

## Results and Discussion

### NMR structural investigation

**Non-photolysed solutions.** The $^1$H NMR spectra of freshly prepared non-irradiated solutions of compounds **3** in

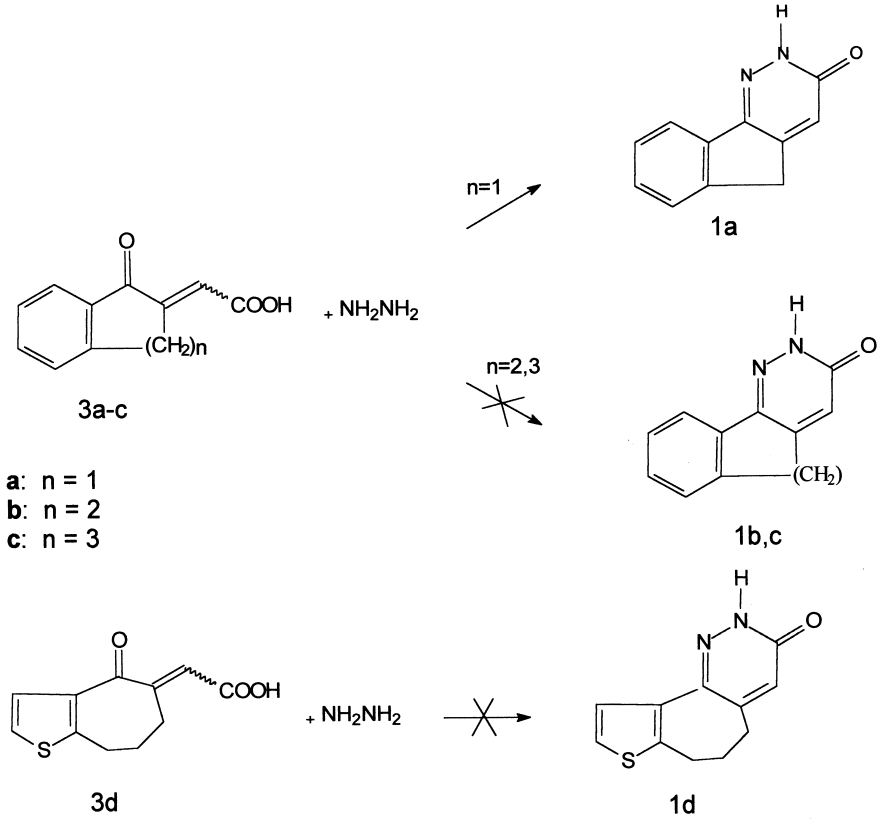


**Scheme 2.**

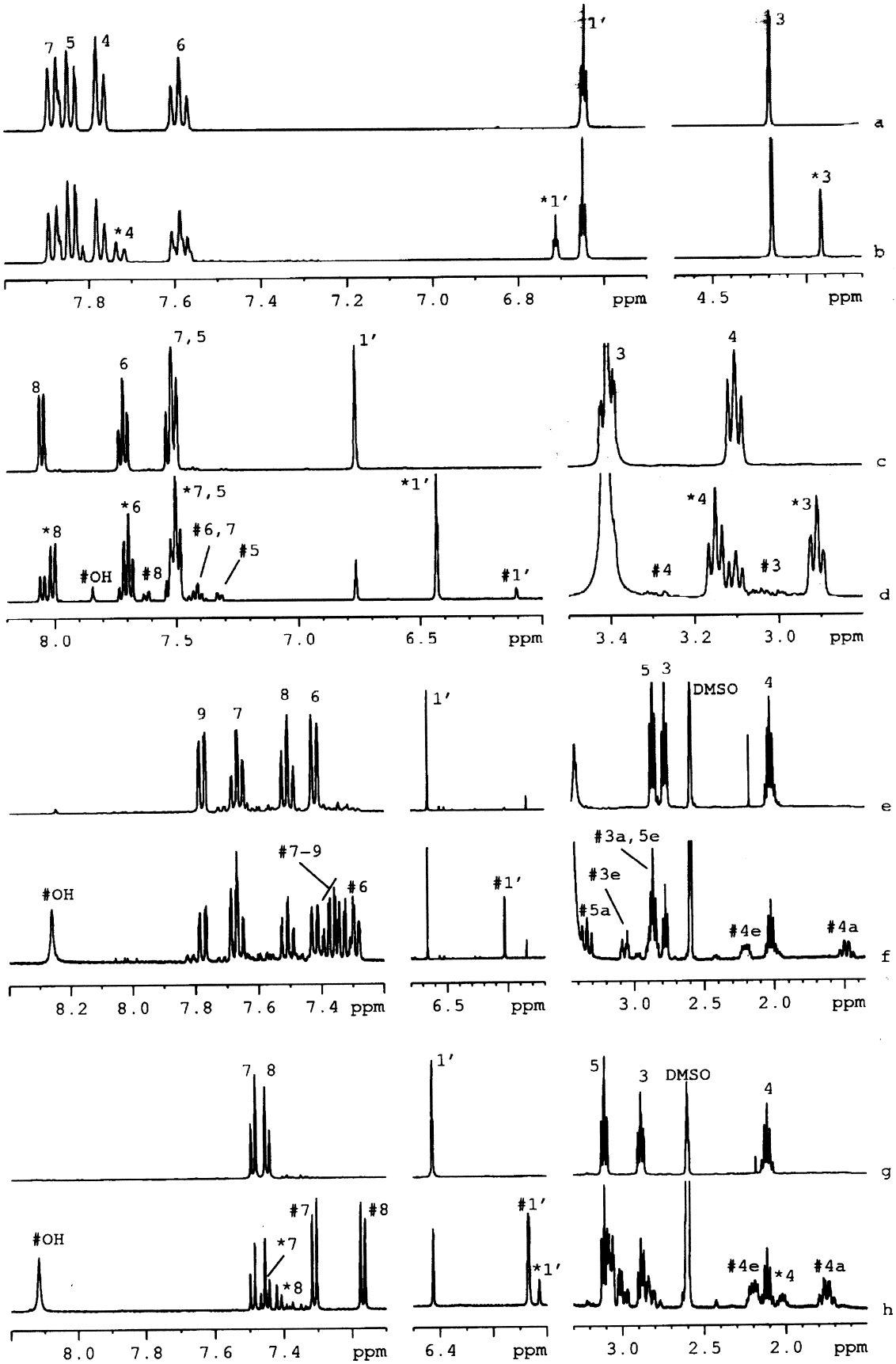


**Figure 1.** $^{1}$H NMR spectra of compounds **3a**–**d**. trace (a) isomer *E*-**3a**; trace (b) mixture of *E*-**3a** (peaks not labelled) and *Z*-**3a** (peaks labelled with *) in molar ratio 100:35; trace (c) isomer *E*-**3b**; trace (d) mixture of isomers *E*-**3b** (no label), *Z*-**3b** (peaks labelled with *) and **6b** (peaks labelled with #) in molar ratio of 30:100:10; trace (e) isomer *E*-**3c**; trace (f) mixture of isomers *E*-**3c** (peaks no labelled) and **6c** (peaks labelled with #) in molar ratio of 100:100; trace (g) isomer *E*-**3d**; trace (h) mixture of isomers *E*-**3d** (peaks no labelled), *Z*-**3d** (peaks labelled with *) and **6c** (peaks labelled with #) in molar ratio of 40:20:100.

DMSO-$d_6$ (Fig. 1, traces a, c, e and g) show that only one species is present in each solution and the multiplicity of the aliphatic hydrogen signals points to the magnetic equivalence of the methylenic protons bound to the same carbon atom, that is $H_2$3, $H_2$4 and $H_2$5 (see Table 1, data sets *E*-**3a**–**d**). Moreover, NOEs between protons H1′ and H3 appear in the spectra of compounds **3a** and **b**, but not in those of compounds **3c** and **d**. While this indicates a preferential *E* configuration at the double bond in the latter two compounds, doubts still exist as to the configuration at the same double bond in compounds **3a** and **b**: in fact, the calculated distances between H1′ and the two H3 atoms, in both *E* and *Z* isomers of these molecules, are short enough as to give rise to a non-negligible dipole–dipole interaction, and thus to a detectable NOE (values between 3.71 and 4.07 Å, for the *E* isomers, and between 2.30 and 3.39 Å, for the *Z* isomers, were calculated). To resolve this uncertainty, photoisomerisation of compounds **3** around the C2–C1′ double bond was attempted by UV photolysis, following the early reports of this kind of photoreactivity of structurally related β-aroylacrylic acids.[11–13]

**Photolysed solutions.** Following UV irradiation, the $^1$H NMR spectrum of compound **3a** showed a new set of signals (Fig. 1 - trace b, peaks labelled with *) in addition to that previously described (Fig. 1, trace a) in a molar ratio of 30:100. The two sets exhibited the same pattern of spin multiplicity and very small differences in the chemical shifts. Both showed NOE between protons H1′ and H3; however, this was much stronger for the new phototropic

**Table 1.** $^1$H NMR chemical shift ($\delta$, ppm), spin multiplicities, coupling constants (*J*, Hz) and main correlations of signal of compounds **3** and **6** (s=singlet, bs=broad singlet; d=doublet, t=triplet, q=quintet, over=overlapped)

| Peak | *E*-**3a** | | *Z*-**3a** | | Peak | *E*-**3b** | | *Z*-**3b** | | **6b** | |
|---|---|---|---|---|---|---|---|---|---|---|---|
| | 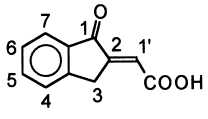 | | 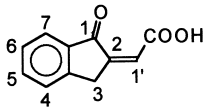 | | | 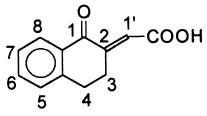 | | 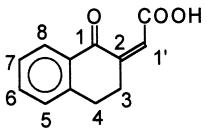 | | 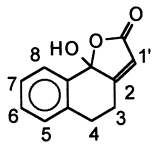 | |
| | $\delta$ | J | $\delta$ | J | | $\delta$ | J | $\delta$ | J | $\delta$ | J |
| H1′ | 6.65 t | 2.2 | 6.71 t | 1.8 | H1′ | 6.77 t | 1.7 | 6.43 t | 1.5 | 6.10 d | 1.5 |
| $H_2$3 | 4.17 d | 2.2 | 3.92 bs | – | $H_2$-3 | 3.41 td | 6.6, 1.7 | 2.99 td | 6.6; 1.5 | 3.05 m | Over |
| | | | | | $H_2$-4 | 3.10 t | 6.6 | 3.15 t | 6.6 | 3.30 m | Over |
| H4 | 7.77 d | 7.8 | 7.72 d | 7.8 | H5 | 7.53 m | Over | 7.53 m | Over | 7.32 dd | 7.4; 1.2 |
| H5 | 7.85 t | 7.8 | 7.830 t | 7.8 | H6 | 7.72 td | 7.9, 1.2 | 7.70 td | 6.1; 1.2 | 7.45 m | Over |
| H6 | 7.58 t | 7.8 | 7.58 t | 7.8 | H7 | 7.51 td | 7.9, 1.2 | 7.59 td | 7.9; 1.2 | 7.45 m | Over |
| H7 | 7.89 d | 7.8 | 7.87 d | 7.8 | H8 | 8.05 dd | 7.9; 1.2 | 8.01 dd | 7.9; 1.2 | 7.62 dd | 7.4;1.7 |
| COOH | 13.10bs | – | 13.16bs | | COOH | 13.00bs | – | 13.00bs | – | – | |
| | | | | | OH | | | | | 7.845 s | – |

*Correlations:* (*E*-**3a**) NOESY: H1′–$H_2$3; $H_2$3–H4; H4–H5; H5–H6; H6–H7; (*Z*-**3a**) NOESY: H1′–$H_2$3; $H_2$3–H4; (*E*-**3b**) NOESY: H1′–$H_2$3; $H_2$3–$H_2$4; $H_2$4–H5; H5–H6; H6–H7; H7–H8; (*Z*-**3b**) NOESY: H1′–$H_2$3; $H_2$3–$H_2$4; $H_2$–H5; H5–H6; H6–H7; H7–H8

| Peak | *E*-**3c** | | **6c** | | Peak | *E*-**3d** | | *Z*-**3d** | | **6d** | |
|---|---|---|---|---|---|---|---|---|---|---|---|
| | 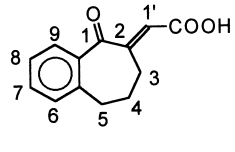 | | 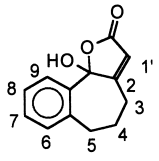 | | | 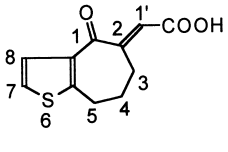 | | 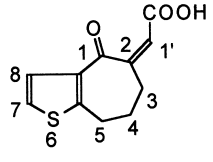 | | 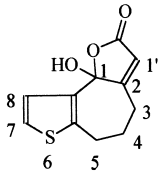 | |
| | $\delta$ | *J* | $\delta$ | *J* | | $\delta$ | *J* | $\delta$ | *J* | $\delta$ | *J* |
| H1′ | 6.66 s | | 6.03 d | 2.0 | | 6.40 s | | 6.03 t | Over | 6.06 d | 1.6 |
| $H_2$3 | 2.78 t | 6.5 | (a) 3.08 dt | 14.3; 3.2 | | 2.88 t | 6.8 | 2.60 | Over | (a) 3.08 m | Over |
| | | | (e) 2.86 | Over | | | | | | (e) 2.84tm | Over |
| $H_2$4 | 2.09 q | | (a) 1.49 qd | 13.1;3.3 | | 2.12 q | 6.8 | 2.02 q | | (a) 1.75 qt | |
| | | | (e) 2.21 m | Over | | | | | | (e) 2.20 m | |
| $H_2$5 | 2.87 t | | (a) 3.34 t | 13.3 | | 3.10 t | 6.8 | 3.08 | Over | (a) 3.0 ddd | |
| | | | (e) 2.86 | Over | | | | | | (e) 3.08 m | Over |
| H6 | 7.42 dd | 7.6; 0.7 | 7.29 dd | 7.2; 1.5 | | | | | | | |
| H7 | 7.67 td | 7.6; 1.3 | 7.67 t | Over | | 7.49 d | 5.3 | 7.46 d | 4.9 | 7.31 d | 5.3 |
| H8 | 7.51 td | 7.6; 1.2 | 7.35 m | Over | | 7.43 d | 5.3 | 7.41 d | 4.9 | 7.17 d | 5.3 |
| H9 | 7.78 dd | 7.6; 1.3 | 7.35 m | Over | | | | | | | |
| COOH | 12.12 bs | | | | | 12.95 s | | 12.80 bs | | | |
| OH | | | 8.26 s | | | | | | | 8.12 s | |

*Correlations:* (*E*-**3c**) COSY: H9–H8; H8–H7; H7–H6; $H_2$5–$H_2$4; $H_2$4–$H_2$3; $H_2$3–H1′ — NOESY: H9–H8; H8–H7; H7–H6; H6–$H_2$5; $H_2$5–$H_2$4; $H_2$4–$H_2$3; **6c**) COSY: H9–H8; H8–H7; H7–H6; H5a–H5e; H5a/e–H4a/e; H4a–H4e; H4a/e–H3a/e; H3a–H3e; H6–H5e; H3a–H1′; NOESY: H6–H5a; H5a–H5e; H5a–H4e; H5e–H4e; H4a–H4e; H4a/e–H3e; H4e–H3a; H3a–H3e; H3e–H1′; (*E*-**3d**) NOESY: $H_2$5–$H_2$4; $H_2$5–$H_2$3; $H_2$4–$H_2$3; (*Z*-**3d**) NOESY: $H_2$5–$H_2$4; $H_2$5–$H_2$3; $H_2$4–$H_2$3; **6d**) NOESY: same as compound 6c

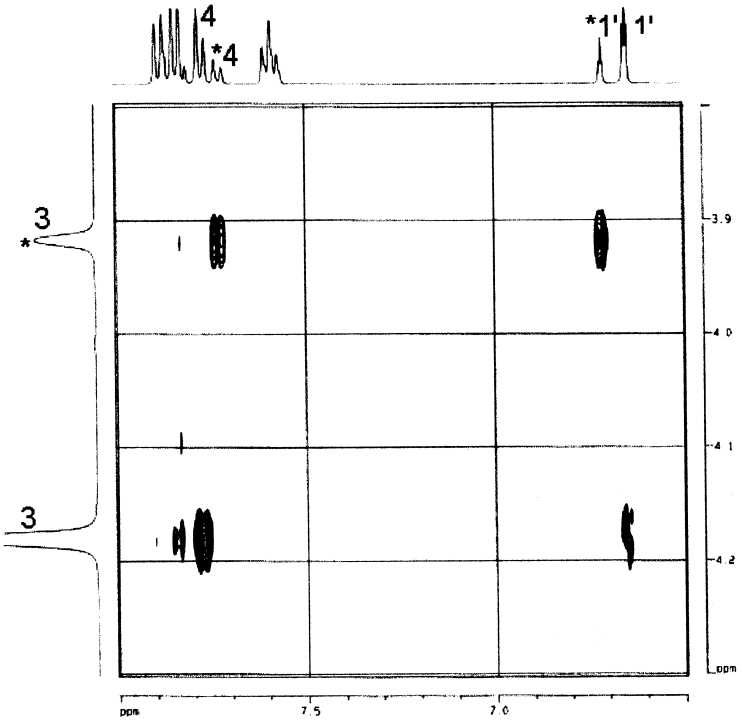


**Figure 2.** NOESY spectrum of the mixture of *E*-**3a** (peaks no labelled) and *Z*-**3a** (peaks labelled with *) in molar ratio 100:35, in the region of H1′–H3 NOEs.

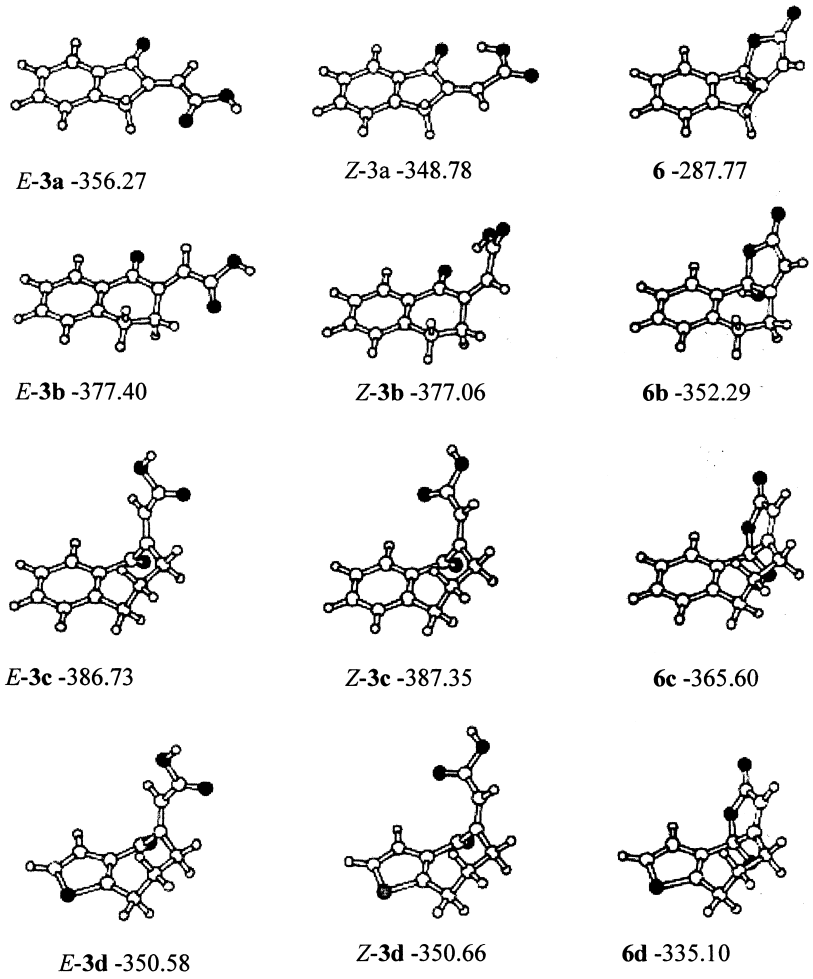


**Figure 3.** 3D plots and heats of formation (kJ $mol^{-1}$) of the minimum-energy conformations of the *E* and *Z* isomers of compounds **3** and of the cyclic compounds **6** obtained by PM3 calculations.

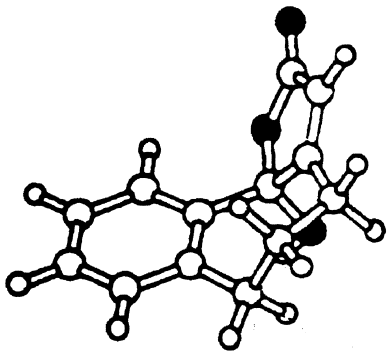

6c

**Figure 4.** Minimum-energy conformations of the cyclic compounds **6c**, obtained by PM3 calculations, with NOEs observed in NOESY spectrum.

species than for the initial one, even though the latter was present in higher concentration (Fig. 2). This suggests a decreased distance between the two hydrogen atoms in the photoproduct and the identification of the starting and photochemically produced species as, respectively, the *E* and *Z* isomers (*E*-**3a** and *Z*-**3a** in Table 1 and in Fig. 3). The $^1$H NMR spectrum of compound **3b** shows, after irradiation, three sets of signals having relative intensities 30:100:10 (shown with no label, asterisk and # in trace d of Fig. 1, respectively). The first two have patterns and NOEs (not shown) similar to those found for compound **3a** and can thus be assigned to the *E* and *Z* isomers (*E*-**3b** and *Z*-**3b** in Fig. 3), the latter being a photoproduct. The third set of signals differs from the other two in that the $H_2$3 and $H_2$4 signals appear as complex multiplets, suggesting loss of magnetic equivalence of the methylenic protons bound to the same carbon. This feature is accounted for by the hemiacetalic structure **6b** (see Fig. 3 and Table 1), as it contains a new chiral centre (C1) which makes the methylenic hydrogen bound to the same carbon atoms diastereotopic. Also, a new singlet, appearing at 7.84 ppm, can be assigned to the hydroxylic hydrogen atom. NOE was not detected with **6b** because the concentration of this species is too low.

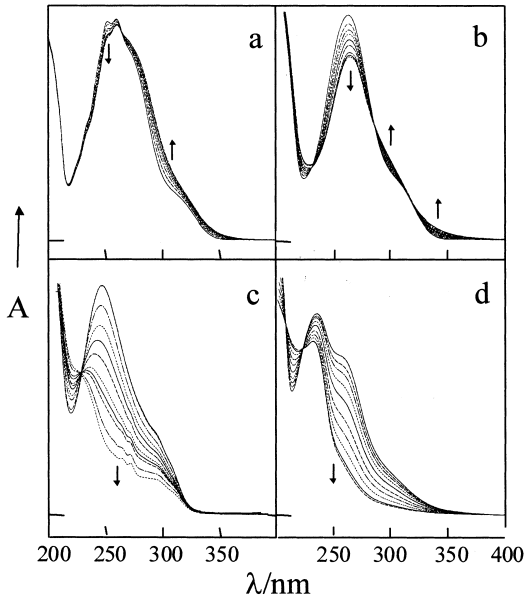


**Figure 5.** Changes in the UV–visible absorption spectra of compounds **3a**–**d** in acetonitrile caused by photolysis with the 313 and 365 nm mercury-lamp lines. The directions of spectral evolution with irradiation time are indicated by arrows. The sample concentrations (mol $l^{-1}$), maximum absorbances in 2 mm cuvettes and total irradiation times (minutes) were as follows: (a) $4.5\times10^{-4}$, 1.45, 64; (b) $5.7\times10^{-4}$, 1.50, 70; (c) $8.5\times10^{-4}$, 1.65, 175; (d) $6.1\times10^{-4}$, 1.50, 132.

For the sake of completeness, compounds **3c** and **3d** were also studied after UV irradiation. The $^1$H NMR spectrum of compound **3c** showed a new set of signals (labelled with # in trace f of Fig. 1) in addition to the one previously described and assigned to the *E* isomer. The relative intensities of the two sets of signals were 90:100. In the new set, the signals of protons $H_2$3 and $H_2$4 appeared as complex multiplets, suggesting a loss of magnetic equivalence of these hydrogens, and a singlet appeared at 8.26 ppm. Similarly to the case of **6b**, these features can be assigned to the hemiacetalic product **6c**. Moreover, the NOEs, the coupling pattern and the values of the coupling constants (Table 1) all support this assignment (Fig. 4).

Finally, the $^1$H NMR spectrum of the photolysed solution of compound **3d** shows three sets of signals with relative intensities 40:20:100 with (respectively no label, asterisk and # in trace h of Fig. 1). An analysis similar to that described for compounds **3b** and **c** leads to their assignment, respectively, as the *E* and *Z* isomers (*E*-**3d** and *Z*-**3d**), and the hemiacetalic structure **6d**, the latter two being the photoproducts. It is relevant to the mechanism of formation of the hemiacetalic forms to observe that, whenever checked during photolysis the ratio of *Z* to **6** forms were independent of time and of the irradiation dose. This suggests that, in all cases, the two forms equilibrate with each other in times of the order of few minutes or shorter.

## Evolution of the UV–visible absorption spectra upon photolysis

Indications in full agreement with the previously described conclusions about the structures of the starting species and the photoproducts come from the analysis of the changes in the UV–visible absorption spectra of compounds **3** brought about by UV photolysis (experimental details are provided in the corresponding section). Irradiation of **3a** in acetonitrile (the reason for the choice of this solvent is given in the Experimental section) caused the spectral changes shown in Fig. 5a. The absorption band evolved to a nearly photostationary spectrum quite similar to the starting one; both maxima were at ca. 262 nm, but the shoulder at about 275 nm increased upon photolysis so that the band centre moved slightly to the red. An isosbetic point at 266 nm was fairly well preserved throughout irradiation, suggesting that the main process taking place was a photoreversible transformation involving one reagent and either one product or a mixture of rapidly equilibrating products. The same held for compound **3b**, whose spectrum in acetonitrile evolved, upon photolysis, to an almost photostationary spectrum keeping two fairly good isosbestic points at 231 and 288 nm (Fig. 5b). The maximum of the photostationary spectrum was essentially unshifted relative to that of the starting one. The only relevant difference between the UV spectral behaviour of compounds **3a** and **b** is that irradiation of the

latter resulted in a pronounced hypochromism, whereas for the former, a very small increase in the absorption band area (if anything) was caused by photolysis. Both observed spectral evolutions are consistent with the $^1$H NMR-based identification of the photoproducts of **3a** and **b** as, respectively, *Z*-**3a** and a mixture of rapidly equilibrating *Z*-**3b** and **6b**.

The UV spectral evolutions of compounds **3c** and **d** upon irradiation were qualitatively different from those of the first two molecules, but they were similar to each other. In fact, rather than approaching a photostationary state, these two molecules exhibited a progressive bleaching of the main absorption bands. This was particularly evident for **3c** (Fig. 5c) whose band, having a maximum at 248 nm, eventually disappeared leaving a shoulder around 230 nm and two additional features: (i) a structured absorption with peaks at about 265 and 272 nm and a shoulder around 258 nm, typical of alkyl substituted benzene (e.g. *o*-xylene in heptane features two peaks at 263 and 271 nm and a shoulder at 257 nm;[14] *o*-methylbenzyl alcohol in isooctane shows peaks at 264 and 273 nm[15]); (ii) a wavy shoulder between 280 and 330 nm assignable to an impurity since it was left unchanged by photolysis and it was not observed in the spectrum of compound **3d** (a fluorescence analysis confirmed this assignment). Similarly, photolysis of compound **3d** caused a dramatic decrease in the intensity of the initial band (Fig. 5d). The shoulders around 260 and 300 nm disappeared almost completely, while the maximum, initially at 235 nm, lowered and moved to 232 nm. Two isosbestic points, at 208 and 223 nm, were preserved throughout irradiation. The final spectrum is reminiscent of the spectra of substituted thiophenes: e.g. 2,3-dimethyl thiophene in isooctane has a maximum at 233 nm.[16] The observed bleaching of the intense *E*-species band with maximum at 248 nm for **3c** and 235 nm for **3d**, assumed to be a 'conjugation' band, i.e. to arise from an electronic excitation delocalised over a large molecular fragment, is consistent with the change in the hybridisation of the C1 atom from $sp^2$ to $sp^3$, associated with the reduction of the main chromophore to an *ortho*-disubstituted benzene or thiophene. This, in turn, agrees with the conclusion reached from the NMR experiments that the main photoproducts for **3c** and **d** are the hemiacetalic **6c** and **d** species. A pronounced hypochromism, similar to the one associated with the formation of the cyclic **6c** and **d** forms, was observed in the photochemical formation of the cyclic lactone of *cis*-β-benzoyl-β-methylacrylic acid from the *trans* form of the acid, closely related with compounds *E*-**3a**–**c**.[12]

To sum up, compounds **3**, all in the *E* configuration, underwent efficient photoreactions yielding different products: while the *Z*-**3a** isomer was obtained with the compound featuring the five-membered aliphatic ring, the hemiacetalic tricyclic forms **6c** and **d** were the dominant photoproducts with the seven-membered aliphatic-ring compounds. Compound **3b** is intermediate, though closer to **3a**, in as much as its main photoproduct was *Z*-**3b**, but a small

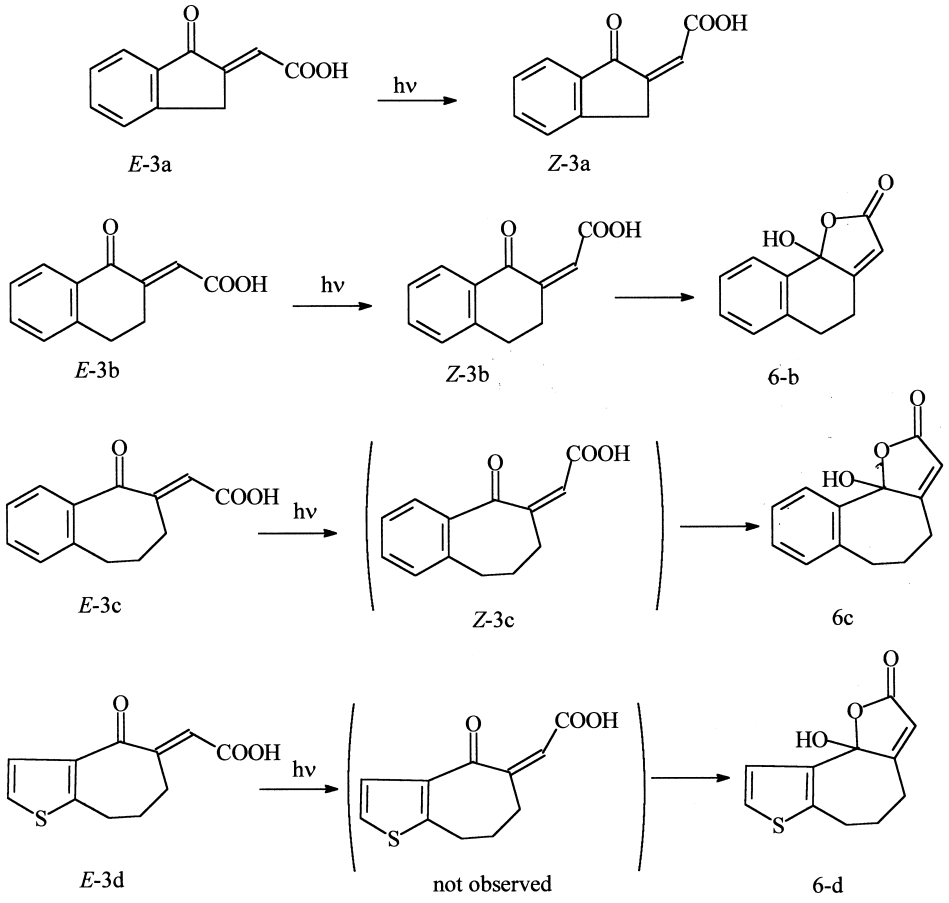


**Scheme 3.**

amount of the cyclic **6b** was also obtained. It is therefore likely that light-induced twisting about the C2–C1′ double bond is operative in all cases but, while the *Z* isomer of **3a** is very stable, those of **3c** and **d** undergo very fast, unobservable cyclisation to the identified stable products **6c** and **d**. A sounder mechanistic analysis of these photoreactions is outside the scope of the present article, and is left for future work. The photoreactivity of **3a**–**d** is summarised in Scheme 3.

## Theoretical analysis of the structures

To explore the relative stabilities of the *E*, *Z* and hemiacetalic forms of compounds **3**, the preferred conformations and the heats of formation of these compounds were theoretically determined using a full geometry optimisation (see the Experimental section for the computational details). Fig. 3 shows the three-dimensional structural plots of the minimum-energy conformations of each compound together with the corresponding heats of formation. Quite interestingly, while compounds *E*-**3a** and **b** are planar or quasi-planar, the two compounds with the seven-membered aliphatic ring are strongly distorted in both *E* and *Z* configurations, with the 'acrylic-acid' moiety almost normal to the phenyl or thiophene plane. This qualitative structural difference is reflected in the absorption spectra of the *E*-**3a**–**c** species: the spectra of the first two compounds are bathochromically shifted with respect to the spectrum of the third one (see the initial spectra in Fig. 5), in keeping with them having more extended, approximately coplanar chromophores. The *E* orientation is the preferred one for **3a**, whereas **3b**–**d** exhibit almost the same heats of formation for the two geometrical isomers. The latter is in contrast with the results of the NMR measurements, which indicate the *E* isomer as the only one present in fresh solutions of all compounds. The contradiction, however, is only apparent because, due to the very high potential-energy barrier for twisting about the exocyclic C–C double bond, the ground-state *E*–*Z* interconversion is extremely slow in the absence of catalysts, as also indicated by the observed stability of the composition of the photolysed samples over several hours or days. Therefore, the dominant presence of *E* species in fresh solutions of all compounds probably results from a stereoselectivity of the route followed to synthesise them, and has little to do with the equilibrium populations of the two isomers. On the contrary, the calculated heats of formation of the **6** forms can be analysed with reference to the ratios of the equilibrium populations of the *Z* and hemiacetalic forms found in the NMR experiments following photolysis because, as previously pointed out, such an equilibration occurs rapidly with respect to the time needed for the measurements. As clearly shown in Fig. 3 the heats of formation of the hemiacetalic forms are systematically lower, in absolute value, than those of the *Z* species. While this result is in keeping with the experimental observations about **3a**, for which no tricyclic form was observed in equilibrium with the *Z* isomer, it cannot account for the low but significant amount of **6b** and the very large amounts of **6c** and **d** observed. The discrepancy might arise from a systematic stabilisation of the hemiacetalic forms relative to the *Z* isomers arising from stronger solvation of the former, an effect not accounted for by the calculations. On the other hand, the observed increasing propensity to give the tricyclic form on going from **3a** to **3b** to **3c** and **d** is qualitatively reflected by the relative order of stability of these forms, in comparison with the *Z* forms, indicated by the calculated heats of formation.

## Reactivities towards hydrazine hydrate

Compounds **3c** and **d**, when reacted with hydrazine in water–acetic acid, yielded a complex mixture of several products each present in small amount, **3a** and **3b**, however, followed clear though distinct reaction pathways: **3a** cyclised to **1a** while **3b** gave a different tryciclic derivative **7b** (Scheme 4). It is reasonable to think that both derive from the same hydrazone intermediate **I** which can cyclise with its $NH_2$ group either on the carboxyl group to give **II**, precursor of **1a**, or on the double bond to give the 2-pyrazoline **III** which, on acetylation of NH gives **7b**. An intermediate similar to **III** has been proposed in the Wolff–Kishner reduction of 2-arylmethylene-1-tetralone.[17,18] To investigate the reasons for the preference of different reaction paths, we performed quantum mechanical calculations (PM3) on **I**, **II** and **III**. Their heats of formation are reported in Scheme 4. Intermediate **IIa** has a lower heat of formation than **IIIa**, whereas the opposite occurs with intermediates **IIb** and **IIIb**. As already indicated by the calculated heat of formation of the hemiacetalic form **6a** (Fig. 3), formation of a tricyclic species with two pentatomic rings, such as **IIIa**, is strongly unfavoured due to severe strain. So, simple thermodynamic considerations might account for the different reaction paths followed by the two compounds. On the other hand, we cannot rule out the possibility that equilibration between reactants **I** and products **II** and **III** be not achieved. Should this be the case, kinetic control would be effective.

## Conclusions

The difference in the observed reactivities of the four 1-oxocycloalkan-2-ylideneacetic acids **3a**–**d** with hydrazine hydrate cannot be traced back to different conformations at the exocyclic C–C double bond. In fact, in freshly prepared non-irradiated solutions, all these compounds are present as *E* isomers. Following photoisomerization to the *Z* forms, differences among the reactivities of the four compounds are observed, with an increasing propensity to give the tricyclic forms **6** with increasing size of the aliphatic ring, likely associated with reduced strain. In particular, compounds **3a** and **b** having smaller aliphatic cycles, can give cyclic products only in the presence of suitable reagents. Reaction with hydrazine hydrate, being probably controlled by the relative stabilities of the intermediates of competitive paths (**IIa** and **b** and **IIIa** and **b** in Scheme 4), cleanly leads to products **1a** and **7b**, respectively. The severe strain in the hypothetical tricyclic derivatives **6a** and **IIIa**, featuring two pentatomic rings, can explain the observed differencies in the results of both photochemistry and reaction with hydrazine of compound **3a** with respect to **3b**. On the other hand, the fast and thermodynamically favoured cyclization of the *Z* forms of compounds **6c** and **d**, featuring a seven-membered aliphatic ring, suggests a general propensity of these compounds to give cyclic products, even without hydrazine hydrate, as

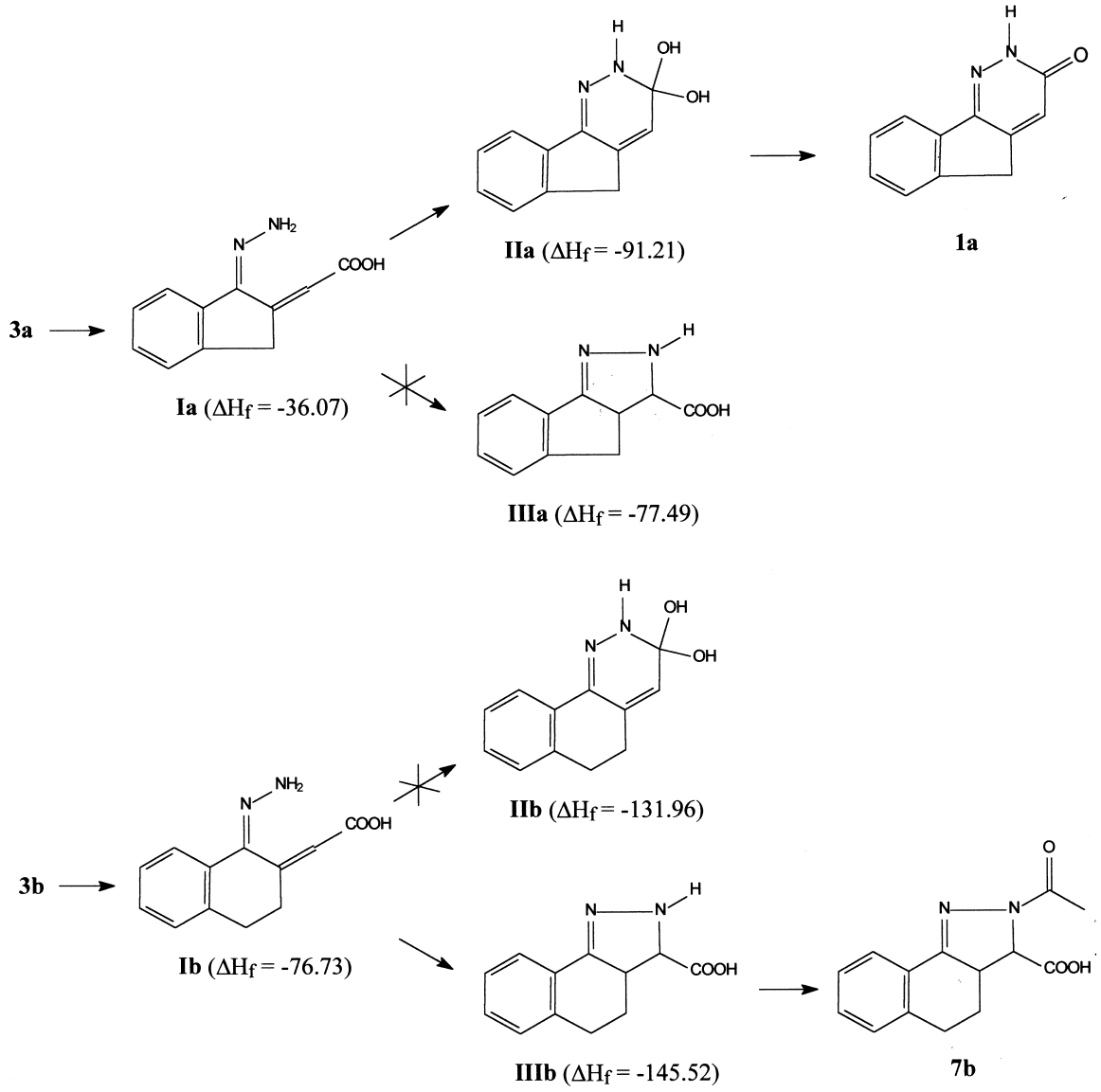


**Scheme 4.**

soon as the *Z* forms are produced in the presence of light, catalysts or under drastic experimental conditions. In this context, replacement of thiophene for benzene does not qualitatively change the observed behaviour. The change along the **3a**–**d** series of the intrinsic propensity for cyclisation is probably responsible for the complex pattern of reactivity towards hydrazine hydrate exhibited by these compounds.

In conclusion, we have shown that such compounds as **3a**–**c**, which differ only in the size of the aliphatic ring, while showing similar photochemical behaviours, exhibit different profiles of chemical reactivity. Rings of different sizes can deeply alter the energetic ranking of the reaction products as well as intermediates. Since constrained analogues of bioactive compounds are often obtained through insertion of a $-(CH_2)_n-$ chain between the correct positions of the parent molecule, care must be paid in the choice of the chain length so as to affect the geometry, but not the stability and the type of reactivity of the obtained compound.

## Experimental

### Reaction with hydrazine

Compounds **3** (1 mmol) were refluxed with hydrazine hydrate (2 mmol) in acetic acid (10 ml) for three hours. After cooling, in the case of **3a**[19] and **3b**[20] a precipitate formed, which was filtered by suction, thoroughly washed with diethyl ether, and then identified from analytical and spectral data as **1a** and **7b**, respectively. On the other hand, with **3c**[20] and **3d**[21] complex reaction mixtures were obtained, in which only traces of the benzo- and, respectively, thiophene-heptapyridazinone were present. **1a**: white-grey powder, mp 298–302°C; $^1$H NMR (DMSO-$d_6$) 4.06 (d, 1.5 Hz, 2H), 7.05 (t, 1.5 Hz, 1H), 7.55 (m, 2H), 7.66 (m, 1H), 7.87 (m, 1H), 12.98 (bs, 1H, exch. with $D_2O$). Anal. calcd C 71.73, H 4.38, N 15.21; found C 71.68, H 4.45, N 15.37. **7b**: white-grey powder, mp>230°C; $^1$H NMR (DMSO-$d_6$) 1.60 (m, 0.68H), 2.00 (m, 0.32H), 2.15 (m, 1H), 2.15 (s, 3H), 3.00 (m, 2H), 3.60 (m, 0.32H), 3.80 (m,

0.68H), 4.40 (d, 10 Hz, 0.32H), 4.95 (d, $J$=10 Hz, 0.68H), 7.36 (m, 3H), 7.88 (m, 1H), 13.00 (s, 1H, exch. with $D_2O$). Anal. calcd C 65.11, H 5.46, N 10.85; found C 64.83, H 5.71, N 11.16.

### $^1$H NMR measurements

All NMR measurements were performed at proton frequency on an AMX-400 WB Bruker spectrometer operating at 9.39 T and equipped with a $^1$H/X 5 mm reverse probehead. All spectra were recorded at 30°C and scaled using the residual signal of the DMSO-$d_6$ peak resonating at 2.6 ppm as the internal reference. Experimental parameters for 1D spectra were as follows: basic spectral frequency=400.130 MHz, spectral width=6400 Hz (14 ppm), time-domain data points: 32 K, pulse width= 3.5 s (45° flip angle), recycle delay=8 s, number of scans=32. FIDs were zero filled to 64 K frequency-domain data points and Fourier transformed without filtering. NOESY spectra were recorded using 2048 time-domain points ($F_2$ dimension) and 512 increments ($F_1$ dimension), 32 scans per increment, TPPI Phase Cycle, a 2400 Hz (6 ppm) spectral width in both dimensions and a mixing time of 400 ms. FIDs were processed doubling the number of point in the $F_1$ dimension and applying a sine square window function (shifted by $\pi/2$ rad) in both dimensions before Fourier transformation.

COSY spectra were recorded using 1024 time-domain points ($F_2$ dimension) and 256 increments ($F_1$ dimension), eight scans per increment and a 2400 Hz (6 ppm) spectral width in both dimensions. FIDs were processed in magnitude mode, doubling the number of point in the $F_1$ dimension and applying an unshifted sine-window function in both dimensions before Fourier transformation.

### Photolysis

Air-saturated solutions of compounds **3** contained in 2 mm optical path cuvettes were irradiated at 365 and 313 nm with a medium pressure mercury lamp filtered through common glass. Such a photolysis arrangement was adopted to the purpose of exploring the photoreactivities of these compounds under the conditions of the synthetic work. The non-monochromaticity of the source made accurate quantum yield measurements unfeasible. Dimethylsulfoxide and acetonitrile were employed as solvents. The former was used to establish a bridge with the $^1$H NMR analysis carried out in this solvent; however, because of its rather high-wavelength absorption onset, it only allowed reliable electronic spectra to be measured above ca. 260 nm. Therefore, photolysis was also performed in acetonitrile which is polar and aprotic like dimethylsulfoxide, but which is transparent down to much shorter wavelengths. The evolution of the whole first intense absorption band of all compounds could be followed in this solvent. That the same photoinduced processes took place in dimethylsulfoxide and acetonitrile was indicated by the close similarity of the spectral changes observed for all compounds in the two solvents at wavelengths higher than 260 nm. The sample concentrations were between 4.5 and $8.5\times10^{-4}$ M in the experiments carried out in both solvents and followed by UV spectroscopy, and from 20 to 100 times larger in the experiments performed in deuterated dimethylsulfoxide and monitored by $^1$H NMR spectroscopy.

### Computational details

Calculations were performed with the PM3 method,[22] implemented in the HYPERCHEM package,[23] and were carried out at the RHF level. The geometry of each compound was fully optimised and energy minimised. Whenever several different starting conformations were possible for a given compound, an optimisation procedure was carried out from each starting geometry, leading to a single absolute minimum in all cases.

## Acknowledgements

This work was supported by the Ministero dell'Università e della Ricerca Scientifica e Tecnologica (MURST, Rome). Technical assistance by M. Bandiera (Modena) is gratefully acknowledged.

## References

1. Holava, H. M.; Partyka, R. A. *J. Med. Chem.* **1971**, *14*, 262–264.
2. Heinisch, G.; Frank, H. In *Progress in Medicinal Chemistry*; Ellis, G. P., West, G. B., Eds.; 1990; Vol. 27, pp 1–49. Heinisch, G.; Frank, H. In *Progress in Medicinal Chemistry*; Ellis, G. P., West, G. B., Eds.; 1992; Vol. 29, pp 141–183.
3. Wamhoff, H.; Korte, F. *Liebigs Ann. Chem.* **1969**, *724*, 217–220.
4. McEvoy, F. J.; Allen, G. R. *J. Org. Chem.* **1973**, *38*, 4044–4048.
5. Robertson, D. W.; Krushinski, J. H.; Beedle, E. E.; Wyss, V.; Pollock, G. D.; Wilson, H.; Kauffman, R. F.; Hayes, J. S. *J. Med. Chem.* **1986**, *29*, 1832–1840.
6. Garcia-Dominguez, N.; Raviña, E.; Santana, L.; Teran, C.; Garcia-Mera, G.; Orallo, F.; Crespo, M.; Fontenia, J.-A. *Arch. Pharmacol.* **1988**, *321*, 735–738.
7. Steck, E. A.; Brundage, P. R.; Fletcher, L. T. *J. Heterocycl. Chem.* **1974**, *11*, 755–761.
8. Lebkucher, R.; Aman, A.; Bachmann, G.; Giertz, H.; Konig, H.; Thieme, P. *Abstracts of Papers 167th ACS National Meeting*, Los Angeles, 1974; MEDI 32.
9. Albright, J. D.; McEvoy, F. J.; Moran, D. B. *J. Heterocycl. Chem.* **1978**, *15*, 881–892.
10. Barlocco, D. Personal communication.
11. Lutz, R. E.; Scott, G. W. *J. Org. Chem.* **1948**, *13*, 284–296.
12. Lutz, R. E.; Bailey, P. S.; Dien, C.-K.; Rinker, J. W. *J. Am. Chem. Soc.* **1953**, *75*, 5039–5044.
13. Sugiyama, N.; Kataoka, H.; Kashima, C.; Yamada, K. *Bull. Chem. Soc. Jpn* **1968**, *41*, 2219.
14. *UV Atlas of Organic Compounds*; Verlag-Chemie: Weinheim, 1966.
15. Entel, J.; Ruof, C. H.; Howard, H. C. *J. Am. Chem. Soc.* **1952**, *74*, 441–444.
16. *Organic Electronic Spectral Data*; Interscience: New York, 1960; Vol. 1.
17. Hartmann, R. W.; Wächter, G. A.; Sergejew, T.; Würtz, R.; Düerkop, J. *Arch. Pharmacol.* **1995**, *328*, 573–575.

18. Wächter, G. A.; Hartmann, R. W.; Sergejew, T.; Grün, G. L.; Ledergerber, D. *J. Med. Chem.* **1996**, *39*, 834–841.
19. Cignarella, G.; Barlocco, D.; Pinna, G. A.; Loriga, M.; Tofanetti, O.; Germini, M. *J. Med. Chem.* **1986**, *29*, 2191–2194.
20. Cignarella, G.; Barlocco, D.; Pinna, G. A.; Loriga, M.; Curzu, M. M.; Tofanetti, O.; Germini, M.; Cazzulani, P.; Cavalletti, E. *J. Med. Chem.* **1989**, *32*, 2277–2282.
21. Barlocco, D.; Cignarella, G.; Fanelli, F.; Vitalis, B.; Matyus, P.; De Benedetti, P. G. *Drug Des. Dis.* **1997**, *14*, 273–290.
22. Stewart, J. J. P. *J. Comput. Chem.* **1989**, *10*, 209–220.
23. HyperChem™ is a package from HyperCube, Inc., Canada.